Continuous acoustic separation in a thermoplastic microchannel

2013 J. Micromech. Microeng. 23 125006

(http://iopscience.iop.org/0960-1317/23/12/125006)

J. Micromech. Microeng. **23** (2013) 125006 (10pp) doi:10.1088/0960-1317/23/12/125006

Continuous acoustic separation in a thermoplastic microchannel

A Mueller, A Lever, T V Nguyen, J Comolli and J Fiering[1]

Charles Stark Draper Laboratory, 555 Technology Square, Cambridge, MA 02139, USA

E-mail: jfiering@draper.com

Received 26 April 2013, in final form 23 August 2013
Published 30 October 2013
Online at stacks.iop.org/JMM/23/125006

Abstract

Acoustic manipulation of particles and cells has been widely used for trapping and separation in microfluidic devices. Previously, the resonant components of these devices have been fabricated from silicon, glass, metals, or other materials having high acoustic impedance. Here, we present experimental results showing continuous acoustic focusing and separation of blood cells in a microchannel fabricated entirely from polystyrene. The efficiency and flow rates approach those reported in silicon and glass systems. We find that the optimum operating frequencies differ from those predicted by conventional approximations which have been developed for more rigid materials. Additionally, we introduce a method for fabrication of the devices, using an adaptation of thermofusion bonding that preserves critical channel dimensions. To control channel cross section during bonding, we introduced a collapsible fiberboard material in the bonding press. This structure provided a self-limiting force and mitigated deformation of the polystyrene. Together, these advances may enable new applications for acoustic focusing and separation in medical devices.

(Some figures may appear in colour only in the online journal)

1. Introduction

Acoustic manipulation of particles, cells, and other suspended objects is a valuable method for concentration, sorting, and separation on the microscale. Termed acoustic focusing, acoustophoresis, or more generally acoustofluidics in recent surveys [1], the method employs the continuous ultrasonic excitation of one or more of the liquid–solid boundaries in a closed microchannel. The resulting time-averaged pressure field in the fluid imparts a velocity to suspended particles, and the ensuing motion may be superposed onto drag or buoyant forces otherwise generated in the microdevice. In acoustic focusing, the particles migrate toward pressure nodes, or in some cases pressure anti-nodes. Because the acoustophoretic velocity is dependent on particle size and material properties, such as the relative density and compressibility of the particle and the fluid medium, differing particles respond accordingly and a mechanism for sorting is available. Several recent publications give excellent analysis of the basic mechanisms of acoustic forces on particles [2, 3].

In microfluidic devices, continuous acoustophoresis may be employed in diverse configurations [4]. Among these are the surface acoustic wave (SAW) device, where actuation of one or more arrays of interdigitated electrodes on a piezoelectric substrate generates a propagating or standing wave along one channel wall's surface [5, 6]. In another approach, which we have adopted, a single bulk transducer is used to excite resonant mechanical modes across the fluid channel, and this may be accomplished in either of the cross section dimensions. For example in an 'out-of-plane' resonator, the primary acoustophoresis occurs parallel to the thickness-mode oscillations of a bulk transducer underneath the channel (i.e., out-of-plane relative to the plane of the transducer and channel substrate). This is typically accomplished by coupling the transducer to the channel base wall and providing a suitable reflecting wall opposite [7–9]. In contrast, for an 'in-plane' resonator, the bulk transducer thickness-mode oscillations excite resonant modes in the perpendicular direction, due to the tuning of channel dimensions and appropriate boundaries at the lateral walls [10–12].

While most biomedical microfluidic devices are fabricated from polymers, acoustophoresis devices have rarely

[1] Author to whom any correspondence should be addressed.

followed this trend. It is evident that to achieve effective focusing, the liquid filled channel and solid walls must form a strongly resonant cavity at some chosen excitation frequency [13]. As a result of this requirement, rigid non-polymer materials such as silicon, glass, ceramics, and metals have been frequently selected [14] because they behave as good acoustic reflectors at the liquid–wall interface. However, particularly for biomedical applications, where the demand for low-cost disposable devices is prevalent, acoustic focusing in plastic is desirable. Another advantage of polymers is that they allow rapid prototyping for developing new designs [15]. Some previously reported acoustic separators use polymers for part of the structure [5, 8, 9, 16, 17], but in these the primary elements of the resonant structure are silicon, glass, or lithium niobate, not polymers. Alternately, acoustophoretic particle concentration has been shown with a metal lens arrangement exciting resonance in a single well of a polystyrene (PS) 96-well plate [18]. There, the polymer served as a reflector in the cavity, but this technique does not appear to have been extended beyond the static well format. In another case, Dron *et al* observed out-of-plane acoustic focusing of microbeads in a channel bounded by plexiglass plates, though apparently at flow velocity of no more than 0.2 mm s^{-1} [19]. Additionally, Gonzalez *et al* reported deflection of 20 μm beads by acoustically exciting the edge of an SU-8 flow cell chip [20].

Another obstacle to acoustic focusing in polymer devices is that precision and consistency in channel dimensions can be critical to constructing an efficient resonator, because the resonant modes are sensitive to dimensions. Embossed thermoplastics can achieve the required precision, particularly when using micromachined templates; however, the bonding of channel layers can lead to inaccuracies due to deformation. Thermoplastic sheets are often bonded by thermofusion (also called thermocompression), which has the benefit that no additional materials (e.g. adhesives) are introduced. Thermofusion bonding has been well documented in the literature [21]. A common challenge in bonding channels by this technique is that the bonding process results in deformation of the channel cross section. As elaborated in the above cited review, many approaches to limiting deformation employ careful tuning of pressure, temperature, and bond time and may also be aided with solvents and surface activation. Recent methods to minimize deformation in adhesiveless bonding include roller lamination [22], chemical surface modification [23, 24], exposure to ultraviolet light [25] and variations of vapor solvent bonding [26].

Microfluidic acoustic focusing and separation in blood and blood cells has been studied in a variety of devices [4, 8, 16, 27–29], and therefore blood is a useful system for characterizing and comparing new acoustofluidic devices. Estimates of relative acoustic forces on the various blood cell types are available [30, 31], and experiments showing discrimination of platelets, erythrocytes, and leukocytes have been performed [29]. In most cases, but not all, e.g. [8], whole blood was diluted to improve separation efficiency. This dilution has been implemented to avoid particle–particle interactions which may reduce acoustic forces and to prevent 'overcrowding' of outlet channels too narrow to accommodate high hematocrit [32].

In this paper we present experimental results showing continuous acoustic focusing and separation of blood cells in a microchannel fabricated entirely from PS, with rates that approach those reported in non-polymer systems. To our knowledge, this is the first demonstration of such performance in an all plastic acoustic flow cell and the first to show in-plane acoustophoresis in a polymer. We find that the optimum operating frequencies differ from those predicted by conventional approximations, presumably because the fluid–polymer interface does not behave as an ideal acoustic reflector. Additionally, we introduce a method for fabrication of the devices, using an adaptation of thermofusion bonding that preserves critical channel dimensions. This method introduces a collapsible fiberboard material between the device and pressure plate, and therefore provides a self-limiting force and mitigates deformation of the PS. This method potentially allows more latitude in how the bonding press is operated. Together, these advances may enable new applications for acoustic focusing and separation in disposable medical devices.

2. Methods

2.1. Materials and design

We selected PS for the polymer flow cell for several reasons. Among polymers, PS has relatively high acoustic impedance and low attenuation at MHz frequencies, according to available materials data [33–37]. A high impedance is desirable for maximum contrast relative to the aqueous contents of the channel. Low attenuation is expected to result in better energy transfer from the transducer and in a higher quality factor in the resonator. Table 1 gives a list of the properties of some of the materials considered. For comparison, the acoustic impedance of silicon or glass, as often used in microfluidic acoustic devices, is around 20 and 12 MRayl, respectively, and for water it is about 1.5 MRayl. These mechanical properties appear to rule out elastomers and many common toughened films and thermoset sheets. Notably, 'filling' polymers with granular additives raises the impedance but also appears to elevate the attenuation in most cases [34]. In addition, we selected PS because it is widely used in biomedical devices and cell culture and is suitable for high volume manufacturing [38]. We also sought good optical clarity for observing the device performance.

The flow cell contained a single microchannel with one inlet and a trifurcated outlet. Of these outlet microchannels, the center outlet channel connected to the first outlet port, and the two edge outlet channels merged into the second outlet port. This outlet configuration allowed us to collect samples from the center stream and the edge streams separately.

The channel dimensions were designed according to design rules given in the analysis by Barnkob [13]. As is well established according to a one-dimensional approximation, to achieve a pressure node along the channel center stream, the channel width was set to one half wavelength of sound

Table 1. Acoustic properties of polymer material candidates. Polymer properties vary by manufacturer and processing; these values are representative only.

Material	Acoustic velocity (m s^{-1})	Density (g cm^{-3})	Acoustic impedance (MRayl)	Attenuation at ~5 MHz (dB cm^{-1})	Reference
Acrylonitrile butadiene styrene	2170–2250	1.03–1.07	2.31–2.36	10.9–11.3	[33]
Acrylic	2750	1.19	2.5–3.26	1.4–7	[33, 34, 36]
Celazole	3430	1.28	4.39	1.8	[35]
Cyclic olefin copolymer	2600[a]	1.02	2.7[a]	–	
Polycarbonate	2300	1.2	2.69–2.75	23.2–24.9	[33]
Polyetheretherketone	2586	1.272	3.24	4.56	[39]
Polyimide	2430	1.42	3.6	–	[37]
Polysulfone	2240	1.24	2.78	4.25	[33]
Polystyrene	2400	1.05	2.52	1.8	[33]
Polystyrene, crosslinked (rexolite)	2340	1.06	2.57	11[b]	[35]
Silicone, transene RTV 141	850[a]	1.3	1.1	14	[34]

[a] Estimated from general mechanical properties.

[b] Measured at 30 MHz.

in the fluid at the nominal operating frequency (however, see Discussion). We took the speed of sound, c, to be 1470 m s^{-1} in physiological saline, and the calculated transducer resonant frequency was 1.71 MHz, based on manufacturer's specifications. We verified this frequency using an LCR meter. These two values dictated a channel width of 430 μm. The channel height was set to 200 μm, a value just below one quarter wavelength in the fluid, which is expected to suppress unwanted out-of-plane modes [14]. As the Barnkob and other studies note, the width of the sidewalls should also be constrained to odd multiples of a quarter wave, using the speed of sound in the wall material. The standard device we tested had a wall thickness (1.05 mm) equal to 3 × the estimated quarter wavelength in PS. The speed of sound was not measured directly, and may vary among varying PS samples, but was taken from literature values to be 2400 m s^{-1} [33]. Other channel dimensions were also selected in alternate devices to investigate resonance behavior and are described in the discussion.

The channel length, L, of 20 mm was selected by estimating a sufficient residence time when flowing across the transducer such that focusing would be complete, meaning that the acoustophoretic displacement would equal at least one half the channel width, or $L = (w\ v_L)/2\ v_w$, where w is the channel width, v_L is the expected average flow velocity, and v_w is the average acoustophoretic velocity. The trifurcation at the downstream end of the device was configured such that the center channel width was 230 μm wide and the two edge outlets were 100 μm wide.

2.2. Fabrication

The flow cell was fabricated using precision conventional machining. The inlet port, outlet ports, and flow channels were machined into 0.95 mm thick sheets ('general purpose' polystyrene, Calsak Plastics, Atlanta, GA, USA), and capped with a second flat sheet (also 0.95 mm) by thermal diffusion bonding. Before sealing, machining debris was removed using isopropanol (IPA) and lint free synthetic wipes. Short lengths of polyetheretherketone (PEEK) tubing, 1/32″ OD and 0.02″ ID, were inserted into the ports and bonded with epoxy (Epoxy 907, Miller-Stephenson, Danbury, CT, USA), and PVC tubing was press fit onto the PEEK stubs for connecting to a syringe pump and outlet sample collection vials. Channel dimensions were verified using digital microscope images at calibrated scale.

We developed a method for thermofusion bonding in a custom pneumatic laminator that prevented deformation of the rectangular channel cross section. The method uses a compressible fiberboard and shims to limit pressure on the heated parts.

The mating sheets were cleaned with IPA and pretreated with oxygen plasma (120 s, 100 W, 30 sccm O_2, 250 mT) in a standard barrel reactor. The two sheets were aligned and placed in the lamination chamber on a 0.005″ thick Kapton polyimide sheet (American Durafilm, Holliston, MA, USA) which serves as a release film. Aluminum square shims, 1.98 mm thick and about 25 mm wide, were placed on either side of the part, and a second Kapton sheet was placed on top. A compressible fiberboard, 1.5 mm thick, (PacoPad, Pacothane Technologies, Winchester, MA, USA) was placed on the stack. Figure 1 shows a sketch of the stack in cross section. The lamination pressure plate applies pressure to the stack. A bond time of 5 min at 96 °C was chosen as a balance between the two limits of flow channel deformation and poor adhesion. Pressure was applied before heating began, and was released after 5 min at temperature. The device was cooled to 80 °C or less before removal from the bond chamber.

The gauge pressure on the upper face of the pneumatically-driven pressure plate was set to 240–275 kPa, while the bottom face is at atmosphere. Because the area of the plate is larger than the area of the device and shims, a pressure amplification results on the surface of the device and shims. Taking into account this amplification, the average pressure on the PacoPad is calculated to be 2.0–2.3 MPa. This pressure is supported by the Al shims and the devices through the compressed fiberboard above them. The actual pressure on the devices is less than on the shims, because the fiberboard is compressed less. Moreover, the duration of applied pressure is limited because the fiberboard plastically deforms as the pressure plate moves to its final position. Using data supplied by the fiberboard manufacturer indicating the % compression of the fiberboard at various pressures, and measuring the initial

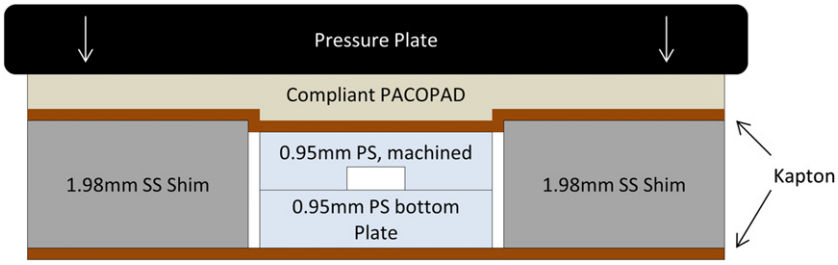

Figure 1. Diagram of thermofusion bonding apparatus showing deformation of the PacoPad fiberboard as pressure is applied. The parts to be bonded are placed between sheets of polyimide release film. Al shims and the fiberboard limit the travel of the pressure plate. The plastically compressed fiberboard transmits pressure to the heated parts to perform the bond. Drawing is not to scale.

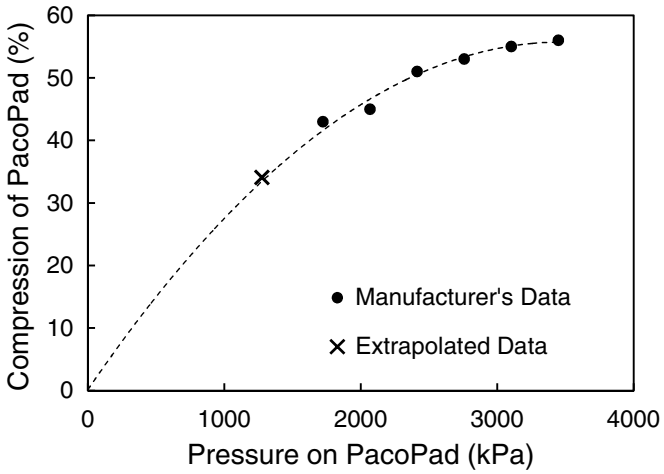

Figure 2. Actual pressure on bonded parts is determined by extrapolating a second order polynomial function fit to the fiberboard manufacturer's compression data. The pad compression in the region bearing on the flow cell was measured before and after bonding.

and final thickness of the board, we calculate the pressure on the device as approximately 1.28 MPa as shown in figure 2.

2.3. Test apparatus

The flow cell was mounted to an acoustic transducer, drive system, and control instruments (figure 3). This apparatus follows closely that reported by Augustsson *et al* [10]. A lead zirconate titanate (PZT) bulk transducer element, 1.2 mm thick and 26 mm in diameter (APC International, PZT 880, Mackeyville, PA, USA) was mounted to an aluminum plate serving as a heat sink. A thin layer of glycerol was added between the transducer and the Al plate to improve heat transport. The heat sink held a thermistor inserted into a small hole filled with heat sink compound and was clamped to the cooled face of a 16 W thermoelectric controller (TEC) element (Laird Technologies, Earth City, MO, USA). A second aluminum plate on the hot face of the TEC acted as a heat exchanger and baseplate. The TEC was regulated by a temperature controller (Wavelength Electronics, Bozeman, MT, USA), typically to 23 °C. A small computer fan was positioned near the test stage to aid the heat exchange.

Sinusoidal output from a standard signal generator was amplified by an RF amplifier (ENI 240L). Voltage at the transducer leads and current were monitored on an oscilloscope. The amplifier featured output protection so that it operated without difficulty despite the poor electrical impedance matching, as the 50Ω output was driving a load of a few ohms at transducer resonance. The transducer had a nominal resonance of 1.71 MHz. The impedance spectrum of the bare transducer and the transducer with a mounted device was measured using a high frequency LCR meter (Hewlett Packard 4395A).

The flow cell was bonded to the transducer using low viscosity cyanoacrylate adhesive. Because the channel was longer than the transducer diameter, trifurcated outlet channels were located beyond the edge of the transducer, though it was not determined if this position is optimal. A syringe pump set the input flow rate, and the syringe was occasionally manually rotated to compensate for particle settling. The flow at the two outlets was constricted by small bore (75 or 100 μm) PEEK capillary tubing, adjusted for inside diameter and length (typically 1–5 cm) such that the average velocity of fluid in the side exit channels was equal to that in the center exit channel. The flow constrictors also served to bias the average pressure in the channel slightly above atmosphere so that outlet flows were insensitive to small changes in elevation. Outlet samples were collected in microcentrifuge tubes and transferred to the analytical equipment. The flow cell and fluid in the channel were observed with an upright microscope having fluorescent and white light illumination, and images were captured on a video camera or a CMOS digital camera.

2.4. Blood and fluid samples

For blood samples, acid–citrate–dextrose anticoagulated human whole blood (Interstate Labs) was diluted to 10 or 20% in phosphate buffer solution (PBS) before loading into syringes. Red blood cell (RBC) counts in outlet samples of 100–300 μL/run were measured by hemocytometer. The hemocytometer depth was 20 μm and counts were averaged from ten locations. Alternately, focusing was observed using 4.5 μm fluorescent carboxylated PS beads (Polysciences) suspended in buffer solution.

3. Results

3.1. Fabrication and bonding

We tested the flow cells for channel deformation due to bonding and for bond strength. Before bonding, the machined

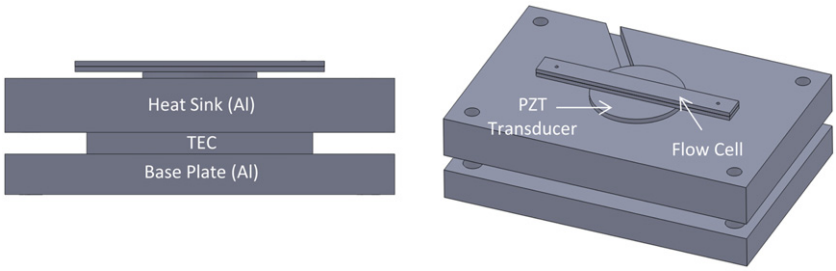

Figure 3. Scale drawing of flow cell mounting to transducer and temperature control stage. From top to bottom the components are: PS flow cell, cyanoacrylate adhesive (not shown), PZT transducer, glycerol layer (not shown), Al heat sink, TEC, and base plate heat exchanger.

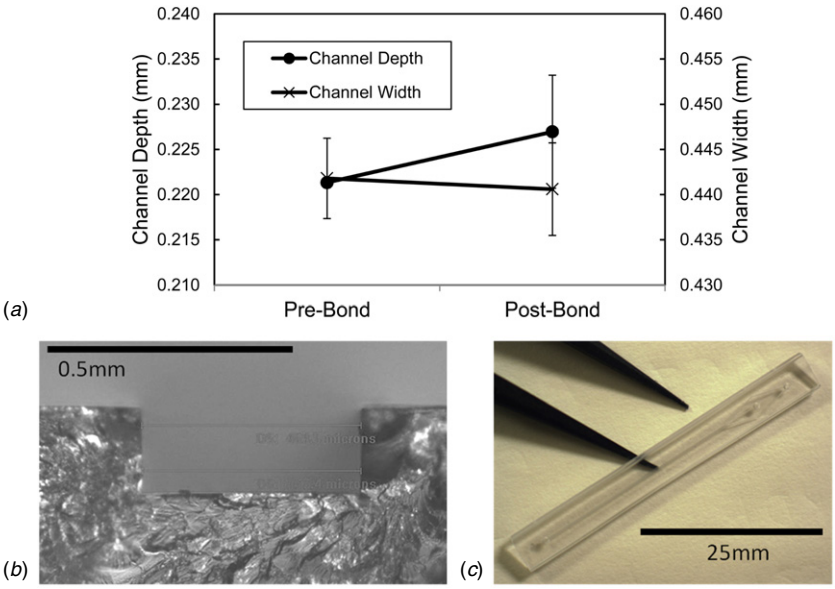

Figure 4. Evaluation of thermofusion bond. (*a*) Plot of channel dimensions before and after bonding. (*b*) Micrograph of cryo-sectioned channel after bonding. Note that cover plate has de-bonded due to sectioning procedure. See text and previous figure for measurements. (*c*) Photograph of completed flow cell.

PS was measured against the nominal dimension of 430 μm for the channel width and 200 μm for the depth. The depth was within 11% of the nominal value and the channel width was within 3%. After bonding, the parts were frozen in liquid nitrogen, cryofractured, and re-measured to verify dimensional consistency. Figure 4 shows that both the channel depth and width were consistent before and after bonding. The more critical dimension of channel width remained within 5% of the nominal value, and changed less than 1% from the pre-bond measurements. These measurements were from two separate runs and each part was measured in at least eight locations. Figure 4 shows a cross sectional image after cryofracturing, confirming that the channels retained the parallel sidewalls important for acoustic focusing. The image shows the open flow channel, without the bonded top plate, since the top delaminates during the freezing and cross sectioning process.

The strength of the bond was characterized using the double cantilever beam test, also known as the razor blade test, which determines the surface energy of the two bonded surfaces. Using this method we determined that the use of oxygen plasma pretreatment increased the bond energy to 300%–400% of the non-treated devices. The final bond energy of the bonded surfaces was approximately 20 N m^{-1}. The operational limits of the bond was tested by filling the channels with PBS and increasing the line pressure using a pressure controller (Alicat Scientific, Tuscon, AZ, USA) until failure. The pressure controller limit of 51 psi was reached without failure of the device. None of the 10–20 devices tested failed due to hydrostatic pressure during ordinary operation.

3.2. Focusing of RBCs

Focusing of red blood cells into distinct streams within the channel flow was observed under a variety of conditions. The focusing was evident by visual observation, as when imaging the channel from above (figure 5). As observed in devices made from more rigid materials, the position and width of the focused streams was dependent on transducer frequency and voltage (figure 6). Furthermore, in control experiments with no signal to the transducer, the cells remained more or less uniformly distributed across the channel width.

Using the diverging outlet channels described above, the system was tuned to concentrate RBCs with optimum efficiency. Frequencies in the range of 0.6–2 MHz were scanned to select a frequency that appeared (by visual inspection) to best focus RBCs to the center of the channel.

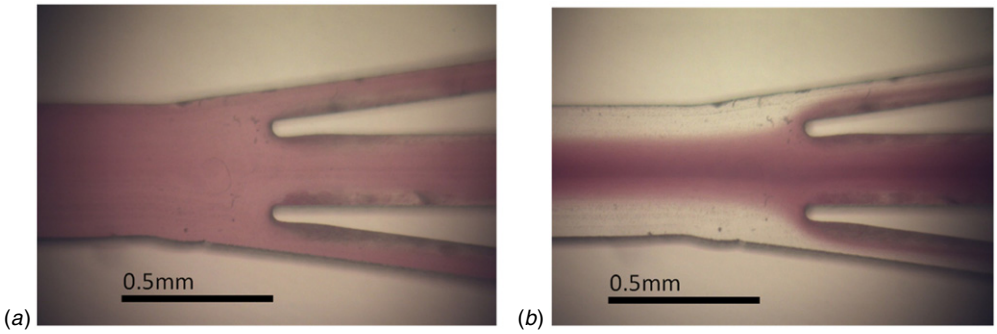

Figure 5. Micrograph showing acoustic focusing and separation of red blood cells at the outlet end of the device. (*a*) Transducer off. (*b*) Transducer on. Solution is 20% human whole blood diluted in PBS. Flow is left to right at 50 μL min^{-1}. Frequency is 1.015 MHz and voltage is 70 Vpp.

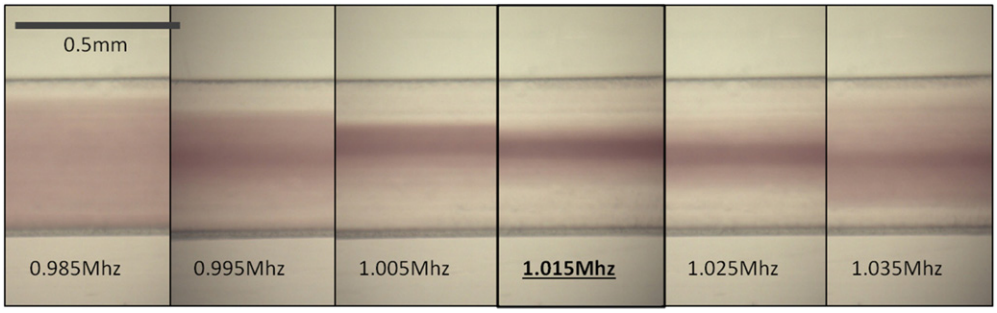

Figure 6. Micrographs showing dependence of focusing on frequency near the observed resonance at 1.015 MHz (underlined). Images show the behavior at the downstream end of the channel. Solution is 10% human whole blood diluted in PBS. Flow is left to right at 100 μL min^{-1}. Transducer voltage is 92 Vpp.

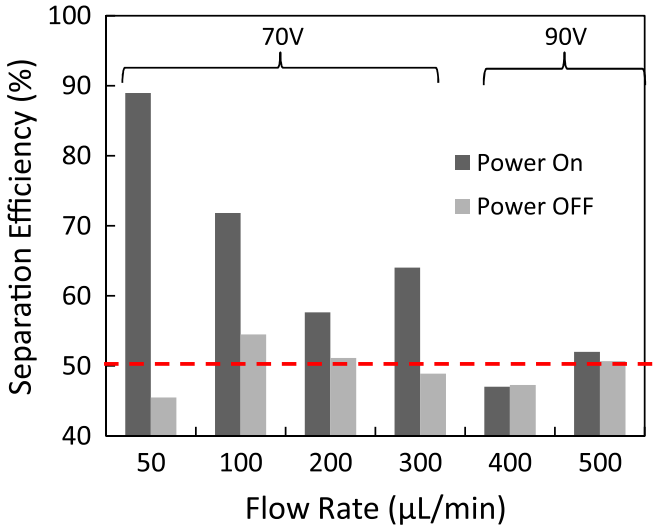

Figure 7. Separation efficiency of RBCs in the center outlet versus flow rate of blood solution. Input solution was 20% HWB diluted in PBS. Excitation was 1.015 MHz. Transducer voltage (peak-to-peak) is shown in the plot, and was increased for the highest flow rates. The dashed line indicates 50% efficiency, equivalent to no separation. Results are plotted with transducer on (dark bars) and, as a control, transducer off (light bars).

This frequency was then held approximately constant as flow rate and/or voltage were varied. At each setpoint combination, we captured 0.1–0.4 ml samples of the outflow and measured RBC concentration. Figure 7 shows the separation efficiency, calculated as [C]/([C] + [E]). Here [C] is the concentration of particles in a sample from the center outlet, and [E] is the concentration of particles in a sample from the combined two edge outlets. Comparing total RBC count before and after flowing through the device, we found trapping or losses in the device to be negligible.

4. Discussion

These results suggest that low-cost thermoplastic devices can perform well to achieve acoustic focusing and separation in blood solutions. When compared with more commonly used silicon and glass devices of similar geometry, the performance metric of capture efficiency versus flow rate is similar. For example, at 300 uL min^{-1}, Petersson *et al* reported 50–60% separation in a 10% blood solution [27]. On the other hand, Adams *et al* recently demonstrated 80–100% separation at rates over 100 $\times$ those reported here, but in a geometry in which cells are deflected perpendicular to the plane of the transducer (out-of-plane), rather than parallel to it [8]. Though this device uses polymer components to simplify fabrication, the primary elements establishing the acoustic resonance are glass plates. In another example, excellent RBC separation efficiency (80–100%) is demonstrated in a SAW device which uses a silicone channel, but the blood flow rate is 0.25 uL min^{-1}, and the resonating substrate is lithium niobate [16]. The good performance of the all-polymer device is perhaps unexpected, given that the acoustic impedance contrast between the fluid and the channel walls is an order

of magnitude less than that of previous devices. A better understanding of the mechanics would aid in further improving design and resulting throughput.

In order to gain preliminary insight into the resonant behavior of this system, we applied a method published by others, in which image analysis of particle density at various stages of focusing was used to estimate the acoustic energy density in the microchannel [40]. This approach measures the relative depletion of particles in regions towards the channel outer walls, away from the focused band, thus ensuring that particle–particle interactions are diminished. This depletion, averaged over many particles, is quantified by a measurement of averaged image intensity in the regions of interest (ROIs). The values are then related to the analytical description of the acoustophoretic displacement, which is dependent on energy density and several constants which are known.

In our case we wished to examine the relative energy density versus frequency using the data shown in figure 6. We excluded the central 30% of the channel width (where particle density is highest due to focusing) and the outermost 10% (where shadowing from channel walls adds artifacts), leaving two ROIs, one in the upper and one in the lower part, of each image. The intensity in these regions was averaged and compared with a maximum value $I_{\max}$ (corresponding to no particles) and to a minimum value (corresponding to a uniform distribution of the input blood solution). Proceeding as delineated in [40], we then applied the relation

$$1 - \frac{I(t)}{I_{\max}} \sim \tan^{-1}\left[A \exp\left(\frac{tE_{\mathrm{ac}}}{B}\right)\right] \tag{1}$$

in which $I(t)$ is the average intensity at the time t in the ROI, A is a constant that depends on the image parameters and ROI definition, B is a constant that depends on the physical properties and dimensions of the fluid channel and particles (including acoustic contrast factor), to solve for E_{ac}, the acoustic energy density. Since all of the images were taken at the downstream end of the channel and at constant flow rate, the time t was the residence time t_{res}, and was constant.

Figure 8 shows the resulting energy densities near the observed resonance. Because of considerable asymmetry in the focusing, we evaluated $I(t_{\mathrm{res}})$ using both of the ROI in each case, and then repeated the evaluation using only the upper or lower ROI. As demonstrated in Barnkob *et al* [41], the relative E_{ac} versus frequency f should follow a Lorentzian function and may be written

$$E_{\mathrm{ac}}(f) = \frac{E_0}{\left[\frac{2Q}{f_0}(f - f_0)\right]^2 + 1}. \tag{2}$$

Hence, figure 8 also shows a plot of this function, fit to the average of the three experimental values at each frequency. The fit uses a center frequency f_0 of 1.016 MHz and Q of 41. The data and the function have all been scaled by the same scale factor such that E_0, the energy density at resonance, is unity.

The absolute value of the energy is not rigorously determined here, because only estimated values of acoustic contrast factor (~0.1) [30], particle diameter (~7 μm), viscosity (~0.01 poise), and residence time (~1.14 s) were

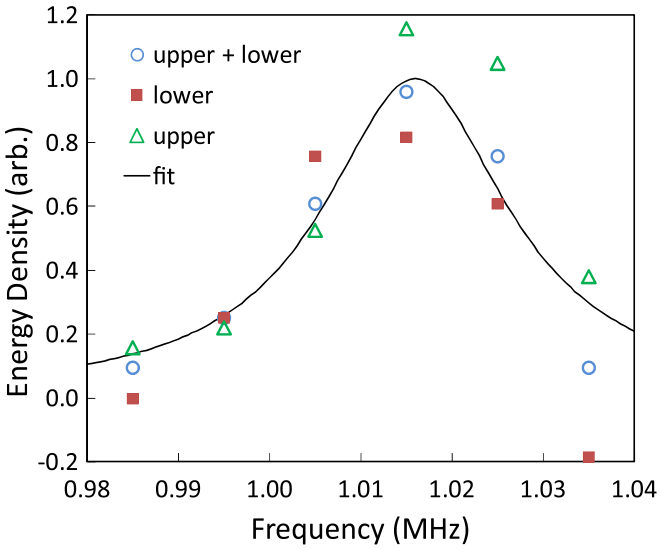

Figure 8. Relative estimated acoustic energy density versus frequency using image analysis from figure 6. The symbols indicate the result of analyzing the RBC density at (○) both the upper and lower portions in the top view of the channel, (■) only the lower half, or (Δ) only the upper half. The solid line is a Lorentzian function (equation (2)), fit to the average of the three symbols.

available for the calculation. Furthermore, the image intensity method is more accurate if numerous time points can be analyzed as the focusing progresses, whereas in our case only a single time point was used. However, as a validation, using the full form [40] of equation (1) with the best available estimates for the experimental constants, we calculate peak energy density of about 20 J m^{-3} which is in reasonable agreement with measurements and calculations by others for similar systems [40–42].

We note with interest that we obtained the most stable focusing and consistent capture efficiency at a resonant frequency lower than what the conventional 1D theory predicts for rigid channel materials such as silicon. In that analysis, the wall–fluid interface is considered a good reflector due to a large mismatch in acoustic impedance [13]. The acoustic impedance, the product of density and acoustic velocity, is about 13 times higher in silicon than in water. In our device, the acoustic impedance ratio is less than 2. Hence it may be unsurprising that the behavior differs. Specifically, the flow channel we tested, if made of silicon should resonate and focus cells (across the channel width) at about 1.7 MHz. However, at and near this frequency, we instead found a symmetric mode with two nodes, resulting in the blood cells focusing into two streams. On the other hand, the optimum resonance shown in figures 6 and 8, near 1.0 MHz, appears to be a symmetric mode, with a node at the center, and was reproducible and stable.

To further investigate the resonance behavior in the thermoplastic devices, we constructed similar devices with varying channel widths and tested focusing. We also tested focusing of PS beads in IPA, a fluid whose nominal speed of sound ($c = 1150$ m s^{-1}) is significantly different from saline. Our choices of channel and wall dimensions were somewhat arbitrary and were restricted by the fixturing established for

Table 2. Experimentally observed resonant frequencies at several variations of channel width, wall width, and/or fluid. Total device width in all cases is 2.53 mm. All channels are 0.2 mm deep.

Channel width (mm)	Wall width (mm)	Fluid	Frequency range tested (MHz)	Primary odd mode frequency (MHz)	Primary even mode frequency (MHz)
0.33	1.1	10% HWB in PBS	0.65–1.8	1.55	–
0.43	1.05	20% HWB in PBS	0.985–1.9	1.015	1.723
0.43	1.05	4.4 μm PS beads in IPA	0.985–1.8	1.033	1.76
0.53	1	20% HWB in PBS	0.66–2.08	0.63	1.67
0.53	1	4.4 μm PS beads in IPA	0.66–2.08	0.92	1.64

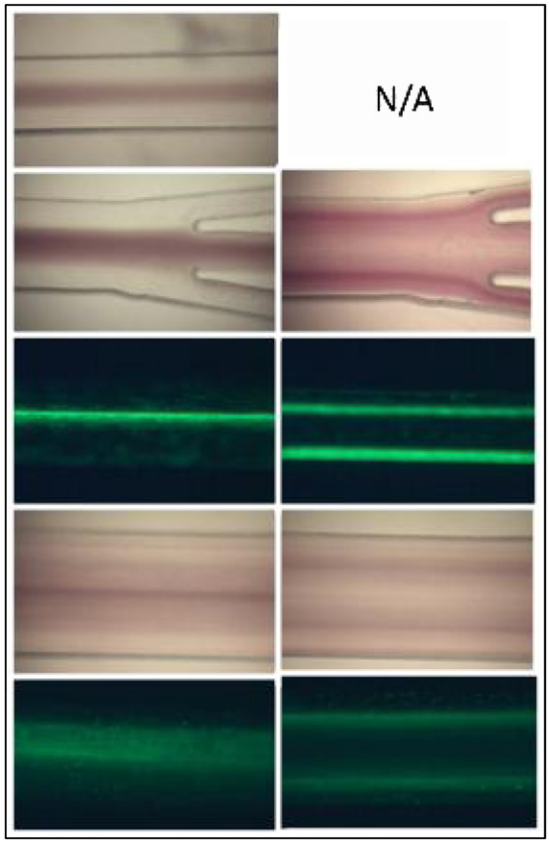

Figure 9. Images corresponding to the observed modes listed in table 2. The left column shows the odd mode and the right column shows the even mode. The devices are, from top to bottom: 0.33 mm channel and PBS, 0.43 mm channel and PBS, 0.43 mm channel and IPA, 0.53 mm channel and PBS, 0.53 mm channel and IPA. Flow in all images is 100 μL min^{-1}.

the primary device. Table 2 and figure 9 show the results of this study. In each case we scanned a frequency range and observed qualitatively the frequency where strong and stable focusing in a center stream occurred. If a dominant double node (even mode) was observed, we noted this frequency as well.

None of the observed behavior agrees with 1D approximations, nor does it appear to agree with a model that ignores the fluid and approximates the device as a block of PS. It is beyond the scope of this paper to undertake an analysis of the resonance behavior of these devices, but the data presented will be useful in developing this in the future. Barnkob and Bruus [13] have emphasized how a multi-dimensional model is needed to thoroughly predict focusing phenomena, and they have also shown that the wall widths and channel width interact. We anticipate that such a model is needed here.

5. Conclusion

A microfluidic acoustic separator was constructed having channels entirely of conventional thermoplastic polystyrene. The device effectively separates RBCs from blood at flow rates comparable to that reported in silicon and glass channels, and with efficiency as high as 85%. Resonant channels made of plastic for focusing have rarely been reported previously, and none have achieved the throughput we observed. These results may enable new applications for acoustic microfluidic systems where low production cost and rapid prototyping is advantageous. To preserve channel dimensions according to design targets and with minimum deformation, we modified common thermocompression bonding by incorporating a fiberboard compression material and rigid shims, preventing excess strain and reducing the duration of the applied mechanical pressure. The separation results reported here were obtained using flow cells fabricated by this approach.

The demonstrations we describe provide a starting point for further development of plastic acoustofluidic devices. While these results already are sufficient for some applications, one can envision further investigation and improvements. It is uncertain to what degree and by what specific mechanisms performance is limited by the material properties of plastic when compared with conventional materials. In particular a better understanding of the relative contribution of acoustic impedance and attenuation would permit designers to choose a polymer accordingly. A combination of additional experimental research, numerical simulations, and fundamental analysis will lead to improved polymer acoustic microfluidics.

Acknowledgments

This material is based upon work supported by DARPA and SSC Pacific under contract number N66001-11-C-4187. We are grateful to Dale Larson and Shivshankar Sundaram for program management. We thank Amy Duwel, Rachelle Prantil-Baun, and Jonathan Adams for helpful discussions.

References

[1] Bruus H, Dual J, Hawkes J, Hill M, Laurell T, Nilsson J, Radel S, Sadhal S and Wiklund M 2011 Forthcoming lab on

a chip tutorial series on acoustofluidics: acoustofluidics-exploiting ultrasonic standing wave forces and acoustic streaming in microfluidic systems for cell and particle manipulation *Lab Chip* **11** 3579–80

[2] Settnes M and Bruus H 2012 Forces acting on a small particle in an acoustical field in a viscous fluid *Phys. Rev.* E **85** 016327

[3] Bruus H 2012 Acoustofluidics 7: the acoustic radiation force on small particles *Lab Chip* **12** 1014–21

[4] Laurell T, Petersson F and Nilsson A 2007 Chip integrated strategies for acoustic separation and manipulation of cells and particles *Chem. Soc. Rev.* **36** 492–506

[5] Ding X, Lin S-C S, Lapsley M I, Li S, Guo X, Chan C Y, Chiang I K, Wang L, McCoy J P and Huang T J 2012 Standing surface acoustic wave (SSAW) based multichannel cell sorting *Lab Chip* **12** 4228–31

[6] Johansson L, Enlund J, Johansson S, Katardjiev I, Wiklund M and Yantchev V 2012 Surface acoustic wave-induced precise particle manipulation in a trapezoidal glass microfluidic channel *J. Micromech. Microeng.* **22** 025018

[7] Townsend R J, Hill M, Harris N R and McDonnell M B 2008 Performance of a quarter-wavelength particle concentrator *Ultrasonics* **48** 515–20

[8] Adams J D, Ebbesen C L, Barnkob R, Yang A H J, Soh H T and Bruus H 2012 High-throughput, temperature-controlled microchannel acoustophoresis device made with rapid prototyping *J. Micromech. Microeng.* **22** 075017

[9] Hultström J, Manneberg O, Dopf K, Hertz H M, Brismar H and Wiklund M 2007 Proliferation and viability of adherent cells manipulated by standing-wave ultrasound in a microfluidic chip *Ultrasound Med. Biol.* **33** 145–51

[10] Augustsson P, Barnkob R, Wereley S T, Bruus H and Laurell T 2011 Automated and temperature-controlled micro-PIV measurements enabling long-term-stable microchannel acoustophoresis characterization *Lab Chip* **11** 4152–64

[11] Adams J D and Soh H T 2010 Tunable acoustophoretic band-pass particle sorter *Appl. Phys. Lett.* **97** 064103

[12] Nilsson A, Petersson F, Jonsson H and Laurell T 2004 Acoustic control of suspended particles in micro fluidic chips *Lab Chip* **4** 131–5

[13] Barnkob R and Bruus H 2009 Acoustofluidics: theory and simulation of radiation forces at ultrasound resonances in microfluidic devices *Proc. Meetings on Acoustics (Portland, OR)* **6** 020001

[14] Lenshof A, Evander M, Laurell T and Nilsson J 2012 Acoustofluidics 5: building microfluidic acoustic resonators *Lab Chip* **12** 684–95

[15] Nge P N, Rogers C I and Woolley A T 2013 Advances in microfluidic materials, functions, integration, and applications *Chem. Rev.* **113** 2550–83

[16] Nam J, Lim H, Kim D and Shin S 2011 Separation of platelets from whole blood using standing surface acoustic waves in a microchannel *Lab Chip* **11** 3361–4

[17] Norris J V, Evander M, Horsman-Hall K M, Nilsson J, Laurell T and Landers J P 2009 Acoustic differential extraction for forensic analysis of sexual assault evidence *Anal. Chem.* **81** 6089–95

[18] Wiklund M, Toivonen J, Tirri M, Hanninen P and Hertz H M 2004 Ultrasonic enrichment of microspheres for ultrasensitive biomedical analysis in confocal laser-scanning fluorescence detection *J. Appl. Phys.* **96** 1242–8

[19] Dron O, Ratier C, Hoyos M and Aider J-L 2009 Parametric study of acoustic focusing of particles in a micro-channel in the perspective to improve micro-PIV measurements *Microfluid. Nanofluid.* **7** 857–67

[20] González I, Fernández L J, Gómez T E, Berganzo J, Soto J L and Carrato A 2010 A polymeric chip for micromanipulation and particle sorting by ultrasounds based on a multilayer configuration *Sensors Actuators* B **144** 310–7

[21] Tsao C-W and DeVoe D 2009 Bonding of thermoplastic polymer microfluidics *Microfluid. Nanofluid.* **6** 1–16

[22] Jeon J, Chung S, Kamm R and Charest J 2011 Hot embossing for fabrication of a microfluidic 3D cell culture platform *Biomed. Microdevices* **13** 325–33

[23] Sunkara V, Park D-K, Hwang H, Chantiwas R, Soper S A and Cho Y-K 2011 Simple room temperature bonding of thermoplastics and poly(dimethylsiloxane) *Lab Chip* **11** 962–5

[24] Im S G, Bong K W, Lee C-H, Doyle P S and Gleason K K 2009 A conformal nano-adhesive via initiated chemical vapor deposition for microfluidic devices *Lab Chip* **9** 411–6

[25] Hu X, He Q, Zhang X and Chen H 2011 Fabrication of fluidic chips with 1-D nanochannels on PMMA substrates by photoresist-free UV-lithography and UV-assisted low-temperature bonding *Microfluid. Nanofluid.* **10** 1223–32

[26] Ogonczyk D, Wegrzyn J, Jankowski P, Dabrowski B and Garstecki P 2010 Bonding of microfluidic devices fabricated in polycarbonate *Lab Chip* **10** 1324–7

[27] Petersson F, Nilsson A, Holm C, Jonsson H and Laurell T 2005 Continuous separation of lipid particles from erythrocytes by means of laminar flow and acoustic standing wave forces *Lab Chip* **5** 20–22

[28] Dykes J, Lenshof A, Åstrand-Grundström I-B, Laurell T and Scheding S 2011 Efficient removal of platelets from peripheral blood progenitor cell products using a novel micro-chip based acoustophoretic platform *PLoS One* **6** e23074

[29] Petersson F, Åberg L, Swärd-Nilsson A-M and Laurell T 2007 Free flow acoustophoresis: microfluidic-based mode of particle and cell separation *Anal. Chem.* **79** 5117–23

[30] Hartono D, Liu Y, Tan P L, Then X Y S, Yung L-Y L and Lim K-M 2011 On-chip measurements of cell compressibility via acoustic radiation *Lab Chip* **11** 4072–80

[31] Barnkob R, Augustsson P, Magnusson C, Lilja H, Laurell T and Bruus H 2011 Measuring density and compressibility of white blood cells and prostate cancer cells by microchannel acoustophoresis *15th Int. Conf. on Miniaturized Systems for Chemistry and Life Sciences (MicroTAS) (Seattle, WA)* pp 127–9

[32] Lenshof A, Ahmad-Tajudin A, Järås K, Swärd-Nilsson A-M, Åberg L, Marko-Varga G, Malm J, Lilja H and Laurell T 2009 Acoustic whole blood plasmapheresis chip for prostate specific antigen microarray diagnostics *Anal. Chem.* **81** 6030–7

[33] Selfridge A R 1985 Approximate material properties in isotropic materials *IEEE Trans. Sonics Ultrason.* **32** 381–94

[34] Grewe M G, Gururaja T R, Shrout T R and Newnham R E 1990 Acoustic properties of particle/polymer composites for ultrasonic transducer backing applications *IEEE Trans. Ultrason. Ferroelectr. Freq. Control* **37** 506–14

[35] Wang H, Ritter T A, Cao W and Shung K K 2001 High frequency properties of passive materials for ultrasonic transducers *IEEE Trans. Ultrason. Ferroelectr. Freq. Control* **48** 78–84

[36] Sinha M and Buckley D J 2007 *Physical Properties of Polymers* ed J E Mark (Berlin: Springer) pp 1021–31

[37] Hadimioglu B and Khuri-Yakub B T 1990 Polymer films as acoustic matching layers *IEEE Ultrasonics Symp. Proc.* vol 3 pp 1337–1340

[38] Berthier E, Young E W K and Beebe D 2012 Engineers are from PDMS-land, biologists are from polystyrenia *Lab Chip* **12** 1224–37

[39] Carlson J E, Van Deventer J, Scolan A and Carlander C 2003 Frequency and temperature dependence of acoustic properties of polymers used in pulse-echo systems *IEEE Symp. on Ultrasonics* vol 1 pp 885–8

[40] Barnkob R, Iranmanesh I, Wiklund M and Bruus H 2012 Measuring acoustic energy density in microchannel acoustophoresis using a simple and rapid light-intensity method *Lab Chip* **12** 2337–44

[41] Barnkob R, Augustsson P, Laurell T and Bruus H 2010 Measuring the local pressure amplitude in microchannel acoustophoresis *Lab Chip* **10** 563–70

[42] Hill M, Townsend R J and Harris N R 2008 Modelling for the robust design of layered resonators for ultrasonic particle manipulation *Ultrasonics* **48** 521–8